CHEMISTRY
A EUROPEAN JOURNAL

DOI: 10.1002/chem.201000859

Electrochemical Synthesis and Characterisation of Alternating Tripyridyl–Dipyrrole Molecular Strands with Multiple Nitrogen-Based Donor–Acceptor Binding Sites

Alexandra Tabatchnik-Rebillon,[a] Christophe Aubé,[a] Hicham Bakkali,[a] Thierry Delaunay,[a] Gabriel Thia Manh,[a] Virginie Blot,[a] Christine Thobie-Gautier,[a] Eric Renault,[a] Marine Soulard,[a] Aurélien Planchat,[a] Jean-Yves Le Questel,[a] Rémy Le Guével,[b] Christiane Guguen-Guillouzo,[b] Brice Kauffmann,[c] Yann Ferrand,[c] Ivan Huc,[c] Karène Urgin,[d] Sylvie Condon,[d] Eric Léonel,[d] Michel Evain,[e] Jacques Lebreton,[a] Denis Jacquemin,[f] Muriel Pipelier,[a] and Didier Dubreuil*[a]

In memory of Gabriel Thia Manh

Abstract: Synthesis of alternating pyridine–pyrrole molecular strands composed of two electron-rich pyrrole units (donors) sandwiched between three pyridinic cores (acceptors) is described. The envisioned strategy was a smooth electrosynthesis process involving ring contraction of corresponding tripyridyl–dipyridazine precursors. 2,6-Bis[6-(pyridazin-3-yl)]pyridine ligands **2a–c** bearing pyridine residues at the terminal positions were prepared in suitable quantities by a Negishi metal cross-coupling procedure. The yields of heterocyclic coupling between 2-pyridyl zinc bromide reagents **12a–c** and 2,6-bis(6-trifluoromethanesulfonylpyridazin-3-yl)pyridine increased from 68 to 95% following introduction of electron-donating methyl groups on the metallated halogenopyridine units. Favorable conditions for preparative electrochemical reduction of tripyridyl–dipyridazines **2b**,**c** were established in THF/acetate buffer (pH 4.6)/acetonitrile to give the targeted 2,6-bis[5-(pyridin-2-yl)pyrrol-2-yl]pyridines **1b** and **1c** in good yields. The absorption behavior of the donor–acceptor tripyridyl–dipyrrole ligands was evaluated and compared to theoretical calculations. Highly fluorescent properties of these chromophores were found ($\nu_{em} \approx 2 \times 10^4\ cm^{-1}$ in MeOH and CH_2Cl_2), and both pyrrolic ligands exhibit a remarkable quantum yield in CH_2Cl_2 ($\phi_f = 0.10$). Structural studies in the solid state established the preferred *cis* conformation of the dipyrrolic ligands, which adopting a planar arrangement with an embedded molecule of water having a complexation energy exceeding 10 kcal mol^{-1}. The ability of the tripyridyl–dipyrrole to complex two copper(II) ions in a pentacoordinate square was investigated.

Keywords: copper · electrochemistry · N ligands · nitrogen heterocycles · ring contraction

[a] Dr. A. Tabatchnik-Rebillon, C. Aubé, H. Bakkali, T. Delaunay, Dr. G. T. Manh,[+] Dr. V. Blot, Dr. C. Thobie-Gautier, Dr. E. Renault, M. Soulard, A. Planchat, Prof. J.-Y. Le Questel, Prof. J. Lebreton, Dr. M. Pipelier, Prof. D. Dubreuil
Laboratoire de Chimie et Interdisciplinarité: Synthèse, Analyse, Modélisation (CEISAM), UMR 6230
Université de Nantes, UFR des Sciences et des Techniques
2, rue de la Houssinière, BP 92208, 44322 Nantes Cedex 3 (France)
Fax: (+33) 251-12-54-02
E-mail: didier.dubreuil@univ-nantes.fr

[b] Dr. R. Le Guével, Dr. C. Guguen-Guillouzo
ImPACcell, Inserm U991, Centre Hospitalier Universitaire Pontchaillou
35033 Rennes Cedex (France)

[c] Dr. B. Kauffmann, Dr. Y. Ferrand, Dr. I. Huc
Institut Européen de Chimie et Biologie (IECB), CNRS UMR5248 et UMS3033
Université de Bordeaux
2 rue Robert Escarpit, 33607 Pessac Cedex (France)

[d] K. Urgin, Dr. S. Condon, Prof. E. Léonel
Institut de Chimie et des Matériaux Paris Est (ICMPE), UMR 7182
Equipe Electrochimie et Synthèse Organique (ESO)
CNRS Université Paris Est Créteil - Val de Marne
2 rue Henri Dunant, 94320 THIAIS (France)

[e] Prof. M. Evain
Institut des Matériaux Jean Rouxel (IMN), UMR 6502
Université de Nantes, UFR des Sciences et des Techniques
2, rue de la Houssinière, BP 92208, 44322 Nantes Cedex 3 (France)

[f] Dr. D. Jacquemin
Unité de Chimie-Physique Théorique et Structurale (2742)
Facultés Universitaires Notre-Dame de la Paix
Rue de Bruxelles, 61, 5000 Namur (Belgium)

[+] Deceased on June 20, 2010.

Supporting information for this article is available on the WWW under http://dx.doi.org/10.1002/chem.201000859.

Introduction

The synthesis of open chain aza donor–acceptor strands constituted by π-conjugated aromatic sequences has been the focus of intense research in recent years because of their potential in a vast array of fields ranging from medicine to materials science, including mechanical, electrical, electrochemical and optical devices.[1] In this context, alternating π-conjugated polypyrrole strands with a central or terminal aromatic segment are of growing interest to provide materials for precise electrochemical conductivity,[1d,2] light harvesting,[3] supramolecular assemblies[4] and biomedical applications.[5] In particular, pyridyl–pyrrole arrays have been used as valuable models to study hydrogen-bonding interaction in protein or DNA binding sites involving the pyrrole NH group, and intermolecular excited-state double proton transfer (ESDPT) for photoinduced mutagenesis was observed in similar structures.[6] Moreover, polydentate pyrrolic-based ligands have attracted particular interest in coordination chemistry due to their π-acceptor properties and their ability to form metal complexes and coordination polymers with high thermal stability. Specifically, dipyrrolic architectures with a central pyridyl core have emerged as potent chromophores, which have recently been found to display not only high electrical conductivity but also to provide a unique combination of electroactive, coordinative and optoelectronic properties. They thus offer an exceptional prospective as materials for use in chemical power sources and organic light-emitting diodes (OLEDs).[2a]

The few strategies described to produce 3,4-unsubstituted bis(pyrrol-2-yl)arylenes currently require the construction of the heteroaromatic core from a flanked dipyrrole system,[5b,7] transition-metal-catalyzed attachment of preformed pyrrole units to a derivatized aromatic core[2g,8] or tandem pyrrole synthesis on the aromatic core from a linear precursor.[1d,2a–c,e,9] These approaches have typically given limited di(pyrrol-2-yl)arylene ring sequences with variable and almost always low overall yields, even the recent Paal–Knoor alternative proposed by Hansford et al. affording 2,5-bis(1*H*-pyrrol-2-yl)pyridines from homoallylic aryl ketones in a relatively concise reaction sequence.[1d]

We have recently become interested in pursuing the electrochemical synthesis of pyrrole rings from pyridazine precursors as an elegant alternative to the classic chemical reagent based processes (Zn/AcOH) extensively used by Boger et al. to produce a broad range of pyrrolic derivatives of biological interest.[10] While the generality of this approach is not obvious, we have succeeded in effecting the electroreduction-driven ring contraction of several 3,6-substituted pyridazines to the corresponding 2,5-substituted pyrroles.[11] As an extension of this "green" methodology, we report here on efficient access to expanded 2,6-bis[5-(pyridin-2-yl)pyrrol-2-yl]pyridines **1a–c** by electrochemical ring contraction of the corresponding 2,6-bis[6-(pyridin-2-yl)pyridazin-3-yl]pyridines **2a–c** (Scheme 1). These alternating pyrrolic sequences flanked by three pyridine units are useful tools to provide original nitrogen-based donor–acceptor ligands of great interest in both photochemistry and biology.

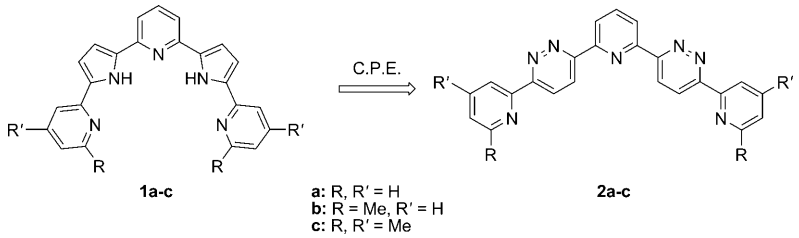

Scheme 1. Electrochemical retrosynthesis of tripyridyl–dipyrrole derivatives from tripyridyl–dipyridazine precursors (C.P.E. = controlled-potential electrolysis).

Results and Discussion

Pyridyl–pyridazine strand synthesis: Our first challenge was the synthesis of alternating tripyridyl–dipyridazine precursors **2a–c** in suitable quantities prior to investigating their preparative electrochemical ring contraction, which was far from established. Lehn et al. previously designed the first and only synthesis of a thirteenfold-alternating *S*-propyl pyridyl–pyridazine sequence bearing bipyridyl groups at the end fragments, and reported their winding into helical architecture **3** (Scheme 2).[12]

The elongation procedure involved construction of the bridging 4-propylsulfanyl–pyridyl moieties by successive condensations of the α-oxoketene dithioacetal unit **4**, used as Michael acceptor, with acetylpyridazine cores **5**/**6** or acetylpyridine **7**. Unfortunately, the extended Potts methodology used[13] led to variable yields at different key steps of the reaction sequence and gave dipyridazinic fragments **5** in quantities too small for electrochemical experiments. We thus turned to a strategy based on metal-catalyzed cross-coupling to prepare tripyridyl–dipyridazines **2a–c** by two alternative pathways (Scheme 3).

Path A, which involves coupling of stannylpyridazines **9a–c** with commercially available dibromopyridine **8**, rapidly appeared to be ineffective. In accordance with literature highlighting the difficult metalation of 3-chloropyridazine derivatives,[14] stannylation of 3-halogeno pyridinyl pyridazines **10a–c**[15] did not exceed 9% yield in our hands. We thus focused on the more promising Path B involving the reaction of metallopyridines **11a–c** or **12a–c** with activated dipyridazines **13** or **14**.

Therefore, the synthesis of the 2,6-di[6-(pyridin-2-yl)pyridazin-3-yl]pyridine derivatives **2a–c** was advantageously pursued from 2,6-diacetylpyridine **15** as a common starting material (Scheme 4).

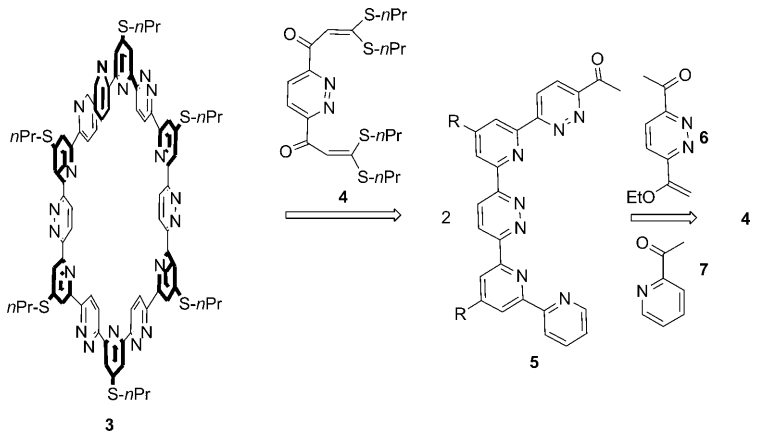

Scheme 2. Retrosynthesis of an alternating pyridyl–pyridazine strand by using the methodology developed by Lehn and co-workers.

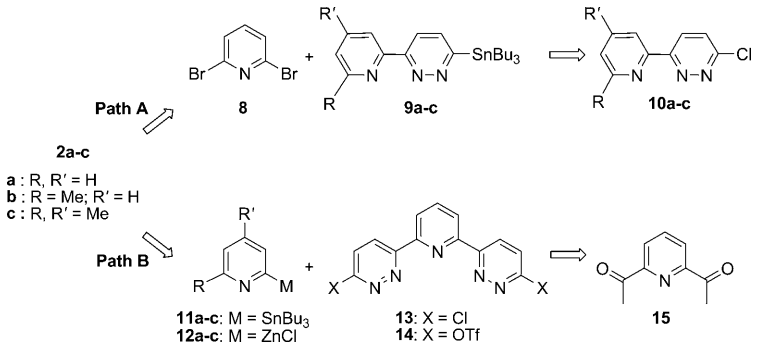

Scheme 3. Retrosynthetic strategy to tripyridyl–dipyridazine precursors **2a–c**.

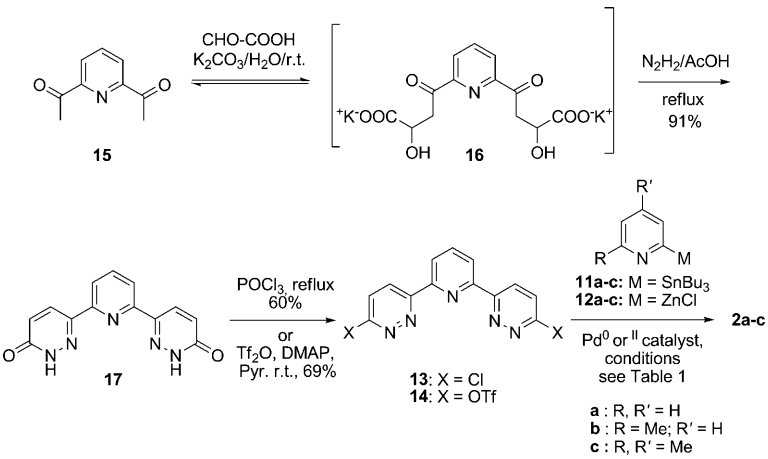

Scheme 4. Synthesis of tripyridyl–dipyridazine precursors **2a–c**.

Diacetylpyridine **15** was treated, following a modified Coates procedure,[16] by condensation with 2.5 equivalents of glyoxylic acid and 4 equivalents of K_2CO_3 in water, prior to addition of an excess of hydrazine in refluxing acetic acid. Under these conditions, the resulting pyridazinone **17** was obtained in an improved yield of 91%. Subsequent chlorination of **17** in refluxing phosphorus oxychloride gave dichlorodipyridazine **13** in 60% yield. Next, Pd-catalyzed cross-coupling reactions between metallopyridine derivatives **11a–c** or **12a–c** and dichloropyridazines **13** were evaluated for formation of dipyridazine targets **2a–c**.

Stille cross-coupling was first attempted with $[Pd(PPh_3)_4]$ as catalyst between chloropyridazine **13** and tributylstannylpyridine **11a**,[17] tributylstannyl methyl pyridine **11b**[17] and tributylstannyl dimethyl pyridine **11c**[17] in DMF at 120°C (Table 1, entry 1).[18] Under these conditions, the formation of stable Pd complexes in the reaction mixtures caused difficulties in the purification procedures that resulted in disappointingly poor yields of dipyridazine derivatives **2a–c** (6–19%). Unfortunately, the use of $[Pd(PPh_3)_2Cl_2]$ as catalyst (Table 1, entry 2) instead of $[Pd(PPh_3)_4]$ did not solve the problem and afforded target dipyridazines **2a**, **2b**, and **2c** in modest yields (trace, 21% and 23%, respectively). Consequently, according to a modified Kasatkin procedure,[19] the Negishi methodology was favored to perform the hetero-cross-coupling reaction of halogenopyridazine **13** with appropriate pyridyl zinc reagents **12a–c**[20] (Table 1, entry 3). The latter were prepared from the corresponding bromopyridines[17b] by treatment with 1.6 equiv of *n*-butyllithium in THF at −78°C for 30 min prior to the addition of zinc dichloride (1.6 equiv). The resulting solutions were stirred from −78°C to room temperature over another 30 min, before the $[Pd(PPh_3)_4]$ catalyst (0.1 equiv) and chloropyridazine **13** (1.0 equiv) were added. The reactions were carried out for 48 h in refluxing THF and the expected dipyridazines **2a**, **2b** and **2c** were cleanly isolated in 13, 45 and 60% yield, respectively. Finally, we found that the triflate analogue **14** (Table 1, entry 4), easily prepared in good yield from pyridazinone **17** (triflic anhydride and catalytic amount of DMAP

Table 1. Conditions of Pd cross-coupling reactions.

Entry	Activated pdz[a]	Pyd-M (2.4 equiv)		Pd catalyst (equiv)	Solvent temp. time	Pdz (%)
1	**13**	**11**	**a**	$[Pd(PPh_3)_4]$	DMF	**2a** (<6)
			b	(0.1)	120°C	**2b** (18)
			c		48 h	**2c** (19)
2	**13**	**11**	**a**	$[Pd(PPh_3)_2Cl_2]$	DMF	**2a** (<2)
			b	(0.1)	120°C	**2b** (21)
			c		48 h	**2c** (23)
3	**13**	**12**	**a**	$[Pd(PPh_3)_4]$	THF	**2a** (13)
			b	(0.1)	reflux	**2b** (45)
			c		48 h	**2c** (60)
4	**14**	**12**	**a**	$[Pd(PPh_3)_4]$	THF	**2a** (27)
			b	(0.2)	reflux	**2b** (68)
			c		48 h	**2c** (95)

[a] Pdz denotes pyridazine.

in pyridine at room temperature, 69% yield), advantageously underwent the desired Negishi coupling reaction with pyridylzinc reagents **12a–c**, and tripyridyl–dipyridazines **2a–c** were isolated in reproducible yields of 27, 68 and 95%, respectively.

In all the organometallic coupling reactions performed, treatment with aqueous ammonia solution (33 wt%) overnight was required to release the pyridazine products trapped in the resulting amalgam. Of course, the low solubility of pyridazine **2a** (R, R′=H) could explain the poor yields obtained in this series. In contrast, the presence of additional methyl groups led to the expected tripyridyl–dipyridazines **2b** and **2c** in proportionally increased yields. Having obtained the dipyridazine precursors in sufficient amounts to carry out electroreduction experiments, we studied their ability to produce the desired tripyridyl–dipyrrole analogues.

Electrochemical ring contraction and pyridyl–pyrrole strand synthesis: In previous studies,[11b–f] we established general favorable conditions for controlled potential electrolysis of 3,6-dipyridylpyridazine derivatives to give the corresponding 2,5-dipyridylpyrroles in acetate buffer/ethanol medium. The electroreduction-driven ring contraction process was shown to be highly sensitive to the nature of the substituents on the pyridazine rings, yielding the pyrrole derivatives in variable proportions. However, in all cases, cyclic voltammetry profiles displayed two well-defined irreversible cathodic peaks and a last wave at a more cathodic potential. These preliminary results allowed us to propose a mechanism involving consumption of four electrons (Scheme 5).[11a]

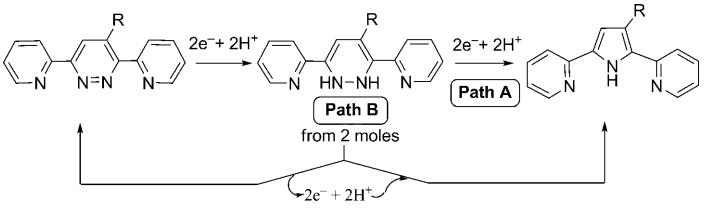

Scheme 5. General electroreduction mechanism for transformation of pyridazine precursors into pyrrole derivatives.

The nitrogen-extrusion sequence starts with formation of dihydropyridazine intermediates (first wave), which evolve to the pyrrole ring by a second electroreduction step (second wave, path A) and/or by a dismutation process (path B). The reduction of the electrogenerated pyrrole derivatives is attributed to the last wave. According to this postulate, the ring contraction of dipyridazines **2a–c** was expected to follow a similar mechanism requiring a minimum of eight electrons (Scheme 6). One question to be answered was which sequence of reduction processes leads to extrusion of the two nitrogen atoms: two independent events at each pyridazine unit or two non-independent consecutive events? Indeed, it was expected that the sequence of reduction processes would influence the electrolysis profile and consequently the yield of dipyrrole formation.

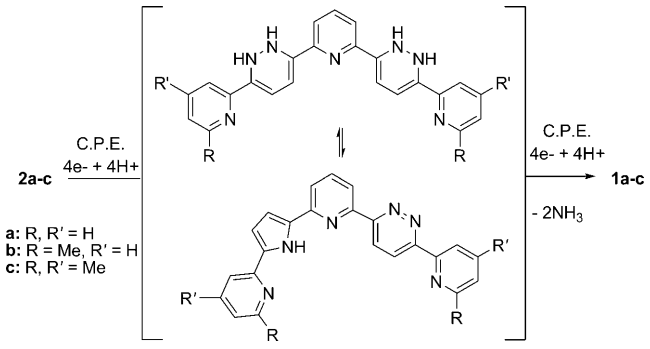

Scheme 6. Electrosynthesis of tripyridyl–dipyrrole derivatives by ring contraction of tripyridyl–dipyridazine precursors.

Poor solubility of the polyheterocyclic systems in acetate buffer/ethanol, previously proven to be an efficient electrolysis medium, could be circumvented by using other buffers. However, the electroreduction study was restricted to dipyridazines **2b** and **2c**, as **2a** appeared quite insoluble in almost all electrolysis solvents tested.[21] Prior to attempting preparative electrolysis experiments, cyclic voltammograms of the dipyridazines were recorded at a glassy carbon cathode in acidic aqueous solvents. The electroreduction profile of **2b** was confirmed in a sulfuric acid (0.5 mol L^{-1}) by the presence of three irreversible cathodic peaks I, II and III at $E_{pc}=-0.53$, -0.68 and -0.85 V, respectively (Figure 1A, Table 2, entry 1).

Based on the analytical data, the controlled potential electrolysis of **2b** was carried out at a mercury-pool cathode in a two-compartment cell with a glass frit. Electroreduction of the dipyridazine **2b** was initiated at the second reduction peak potential (E_{pcII}) at $E_w=-0.9$ V/SCE (Table 3, entry 1) and was monitored by cyclic voltammetry measurements in the cathodic compartment. The shift to the cathodic potentials observed in the cyclic voltammogram (Figure 1B, $E_{pc}=$ -0.55, -0.89 and -1.16 V), was attributed to the increased concentration of the substrate used in preparative electrolysis (7×10^{-3} mol L^{-1} vs. 10^{-3} mol L^{-1} under analytical conditions). A proportionate decrease in the intensity of the two

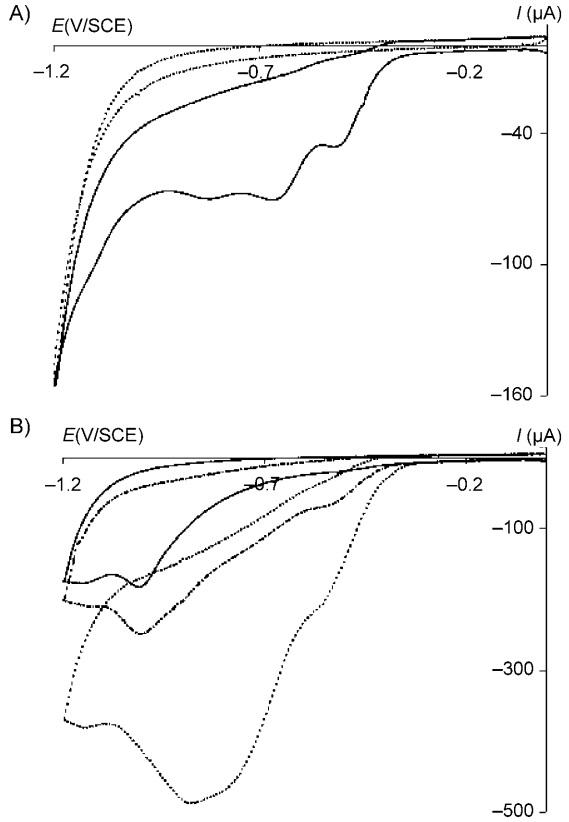

Figure 1. Cyclic voltammograms at a glassy carbon electrode ($v=0.1\,V\,s^{-1}$) of A) $0.5\,mol\,L^{-1}$ H_2SO_4 solution (– – –) prior to addition of **2b** (——, $C=10^{-3}\,mol\,L^{-1}$). B) **2b** ($C=7\times10^{-3}\,mol\,L^{-1}$) in $0.5\,mol\,L^{-1}$ H_2SO_4 before electrolysis (– – –), after $5\,F\,mol^{-1}$ (-----), and after $8\,F\,mol^{-1}$ (——).

Table 2. Cyclic voltammetry data of compounds **2b**, **2c**, **1b** and **1c** ($C=10^{-3}\,mol\,L^{-1}$, E_p [V/SCE] and $v=0.1\,V\,s^{-1}$).

Entry	Solvent	Compound	E_{pcI}	E_{pcII}	E_{pcIII}
1	H_2SO_4	**2b**	−0.53	−0.68	−0.85
2	H_2SO_4	**1b**	–	–	−0.98
3	THF/acetate buffer/CH_3CN	**2b**	−0.96	−1.19	–
4	THF/acetate buffer/CH_3CN	**1b**	–	–	−1.45
5	THF/acetate buffer/CH_3CN	**2c**	−0.94	−1.17	–
6	THF/acetate buffer/CH_3CN	**1c**	–	–	−1.44

main peaks I and II in favor of the reduction peak III ($E_{pc}=-1.02$ V) highlighted the electroreduction evolution of **2b**. The electrolysis was stopped after total consumption of the required $8\,F\,mol^{-1}$, and the starting dipyridazine substrate had disappeared to give the expected tripyridyl–dipyrrole derivative **1b** in an unsatisfactory yield after flash chromatography on silica gel (16%). The electroreduction profile of purified **1b** was controlled to assign the remaining irreversible cathodic peaks at $E_{pc}=-0.98$ V (Table 2, entry 2).

Alternatively, the preparative electrolysis was then carried out in an organic solvent. Due to the poor solubility of **2b** in CH_3CN, DMF was retained as an electrochemically inert solvent, and in that case the addition of a support electrolyte ($0.10\,mol\,L^{-1}$ nBu_4NBr) to achieve conductivity in the medium and a new source of protons (16.0 equiv H_2SO_4) were required. Under these conditions, the cyclic voltammogram revealed five reduction waves that were difficult to interpret (see the Supporting Information). Several preparative electrolyses at various reduction potentials until the consumption of $8\,F\,mol^{-1}$ led to only traces of the expected pyrrole **1b** (Table 3, entry 2). This disappointing result was difficult to rationalize, as the large excess of nBu_4NBr in the reaction mixture imposed a tedious purification treatment that prevented convenient isolation of the final product due to severe loss of material. To solubilize dipyridazine precursor **2b**, we then turned to a mixture of an organic solvent (THF) and an aqueous solution as proton donor, in addition to a supporting electrolyte (acetate buffer pH 4.6). The resulting biphasic solution was homogenized by adding a third, miscible cosolvent to the medium. After several assays, the optimized conditions were defined as THF/acetate buffer (pH 4.6)/acetonitrile in 5:4:1 ratio. Under these conditions, the cyclic voltammogram of dipyridazine **2b** showed only two well-defined reduction waves, at $E_{pc}=-0.96$ and -1.19 V (Figure 2A, Table 2, entry 3). In this voltammogram, a third cathodic wave corresponding to reduction of the pyrrole is also observed but not well enough defined to be measured precisely.

Table 3. Coulometric data and yield of the electrochemical synthesis of pyrroles at a mercury-pool cathode.

Entry	Pdz ($C\,mol\,L^{-1}$)	Solvent	E_w [V][a]	N [$F\,mol^{-1}$]	Pyr[b] [%]
1	**2b** (7.0×10^{-3})	H_2SO_4 ($0.5\,mol\,L^{-1}$)	−0.90	8	**1b** (16)[c]
2	**2b** (2.8×10^{-3})	DMF/nBu_4NBr ($0.1\,mol\,L^{-1}$)/ 16 equiv H_2SO_4	various potentials	8	**1b** (trace)
3	**2b** (4.8×10^{-3})	THF/acetate buffer (pH 4.6)/ CH_3CN (5:4:1)	−1.25	8	**1b** (71)[d]
4	**2c** (1.6×10^{-3})	THF/acetate buffer (pH 4.6)/ CH_3CN (5:4:1)	−1.20	12	**1c** (93)[d]
5	**2c** (1.6×10^{-3})	THF/acetate buffer pH 4.6)/ CH_3CN (5:4:1)	−1.20	12	**1c** (72)[d,e]

[a] E_w: working potential/SCE. [b] Pyr denotes pyrrole. [c] Purified by flash chromatography on silica gel. [d] Purified by crystallization from hexane/chloroform (4:1). [e] Electrolysis was run on a reticulated vitreous carbon cathode.

Preparative electrolysis of **2b** was monitored at $E_w=-1.25$ V/SCE (E_{pcII}, Figure 2B). In the course of electrosynthesis, the appearance of the pyrrole reduction peak was cleanly observed at $E_p=-1.45$ V, in good agreement with the analytical cyclic voltammogram of the pure dipyrrole **1b** (Table 2, entry 4). This encouraging indication was confirmed at the preparative level, since the expected dipyrrole **1b** was formed as the sole product of the electroreduction process after consumption of $8\,F\,mol^{-1}$ (Table 3, entry 3).

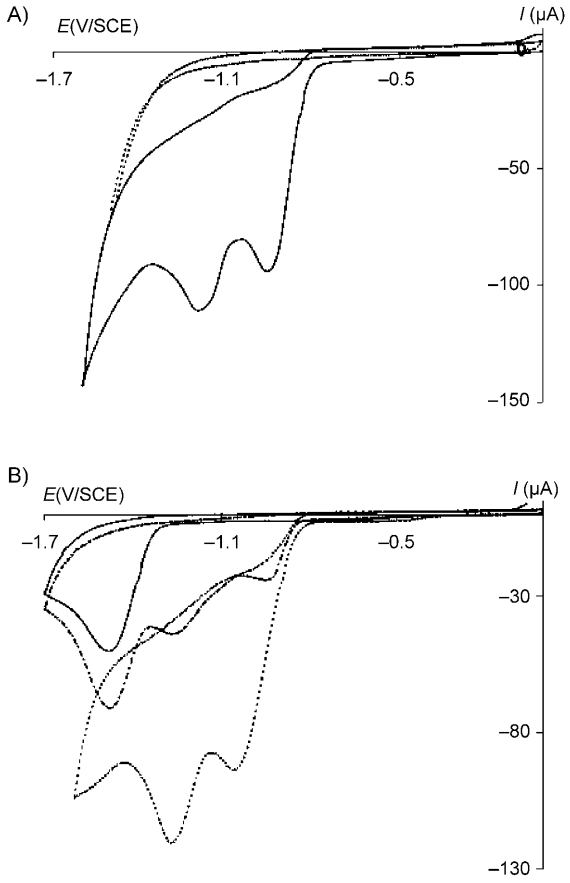

Figure 2. Cyclic voltammograms at a glassy carbon electrode ($v=0.1\,V\,s^{-1}$). A) THF/acetate buffer (pH 4.6)/CH_3CN (5:4:1, – – –) prior to addition of **2b** (——, $C=10^{-3}\,mol\,L^{-1}$). B) **2b** ($C=4\times10^{-3}\,mol\,L^{-1}$) in THF/acetate buffer (pH 4.6)/CH_3CN (5:4:1) before electrolysis (– – –), after 5 $F\,mol^{-1}$ (-----), and after 8 $F\,mol^{-1}$ (——).

Tripyridyl–dipyrrole **1b** was isolated in 71% yield by crystallisation from chloroform/hexane (4:1), whereas it was obtained in a lower yield of 45% after flash chromatography on silica gel. To facilitate a mechanistic interpretation, we envisaged identifying the intermediates by running the electroreduction at the potentials of the two waves and limiting the electron source to 4 $F\,mol^{-1}$. Unfortunately, these experiments led to complex mixtures in which dipyrrole and monopyrrole were identified (see ^1H NMR spectra in the Supporting Information). Inasmuch as no formation of dihydropyridazine was observed along with production of the pyrrole derivatives and remaining dipyridazine precursor, no evidence was obtained to elucidate the process.

The optimized electroreduction procedure was then transposed to tripyridyl–dipyridazine **2c** in the same ternary THF/acetate buffer (pH 4.6)/acetonitrile solution (5:4:1) with the expectation of obtaining the corresponding tripyridyl–dipyrrole **1c**. As anticipated from the analytical voltammogram (Table 2, entry 5), the electrolysis of **2c** was run at $E_w=-1.20$ V/SCE (E_{pcII}, Table 3, entry 4) to afford **1c** in 93% yield after crystallization from chloroform/hexane (4:1). The electroreduction profile of purified **1c** was confirmed by the presence of one irreversible cathodic peak at $E_{pc}=-1.44$ V (Table 2, entry 6). The controlled-potential electrolysis of dipyridazine **2c** was alternatively tested with a reticulated vitreous carbon cathode (Table 3, entry 5), in the solution described above, avoiding the use of mercury. Under these "green" conditions, the desired tripyridyl–dipyrrole **1c** was formed at $E_w=-1.20$ V/SCE in an acceptable yield of 72%.

Absorption and fluorescence studies: The absorption characteristics of alternating tripyridyl–dipyridazines **2b** and **2c** and their dipyrrole analogues **1b** and **1c** were tackled. Previous investigations, through quantum chemistry calculations (HF, DFT (MPWB1K), LMP2 levels of theory), highlighted the planar conformational preferences of both strands, and global energetic minima confirmed the existence of π-electronic conjugation between the aromatic systems and the occurrence of intramolecular H-bonds. Thus, the combination of N sp^2 nitrogen–nitrogen lone-pair repulsion and weak CH···N sp^2 attractive interaction in dipyridazine derivatives **2** results in a preferred *anti* conformation, whereas, more surprisingly, the all-*cis* conformation of tripyridyl–dipyrroles **1** is rationalized by the occurrence of NH···N sp^2 H-bonds involving the central pyridazine core and the two pyrrole units.[22]

The absorption spectra of dipyridazines **2b** and **2c**, recorded in CH_2Cl_2 (Figure 3A), show two similar main bands at 316 and 257 nm for both compounds, that is, additional methyl groups have no effect on the absorption features.

For **2b**, quantum-chemical calculations at the DFT level yield a perfectly planar C_{2v} structure, and TD-DFT foresees a strongly allowed transition at 300 nm that obviously corresponds to the experimental band at 316 nm. This 16 nm discrepancy is in line with the expected accuracy of the selected level of theory.[23] At the PCM-CAM-B3LYP level, the major contribution of this peak corresponds to an electron promotion from the HOMO to the LUMO+1. As can be seen in Figure 4, these π and π* orbitals are delocalized over the full molecule, with the occupied orbital mainly located in the five rings, whereas its virtual counterpart displays a significant contribution on the inter-ring bonds. In addition, theory predicts significant bands at 287 and 263 nm that are consistent with the shape of the experimental band, as well as dipole-forbidden excitations at 306 and 312 nm. These latter absorptions, corresponding to n→π* transitions involving the lone pairs of the pyridazine moieties, remain unseen experimentally as they are too close energetically to the main π→π* band.

Both dipyrroles **1b** and **1c** display a similar absorption profile (Figure 3B) but the nature of the heterocycle at the 2- and 6-positions of the central pyridine shifts significantly the electronic absorption maxima to give two main bands at about 340 and about 380 nm in CH_2Cl_2 with distinct vibrational structures. For **1b**, a twisted C_2 ground state is obtained by DFT simulations (see below for discussion). As illustrated in Figure 3C, the two first calculated absorption maxima are centred at 356 ($f=0.6$) and 324 nm ($f=1.3$) in CH_2Cl_2.

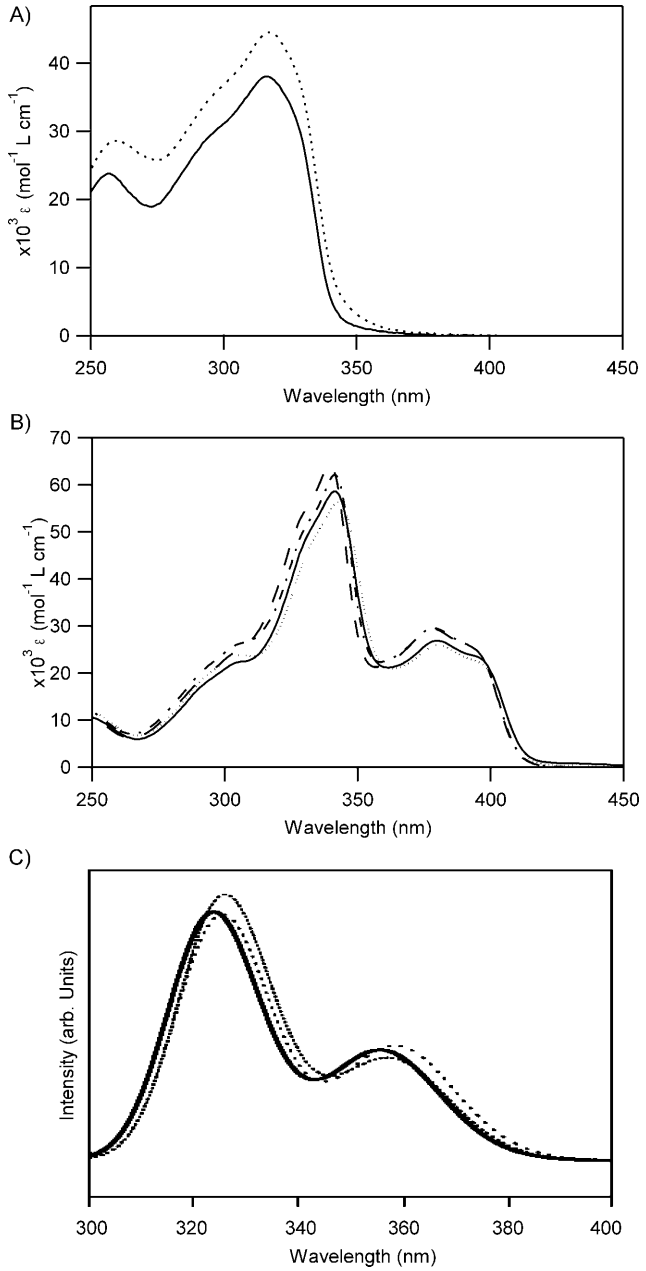

Figure 3. A) Absorption spectra of dipyridazines **2b** (——) and **2c** (•••••) in dichloromethane. B) Absorption spectra of dipyrroles **1b** (•••••), **1c** (——) in dichloromethane, **1b** (-----) and **1c** (– – –) in methanol; C) Simulated absorption spectra of **1b**. The curves [C_2 structure (——), C_{2v} structure (•••••), and C_{2v} structure with central water molecule (•••••)] were obtained at the PCM-CAM-B3LYP/6-311+G(2d,p) level by using a broadening Gaussian with full width at half-maximum of 0.25 eV. Note that the two C_{2v} structures are not true minima of the potential-energy surface and are presented for comparison purposes only.

Though these values are shifted by about 20 nm with respect to their experimental counterparts (Table 4), the agreement between the two schemes is certainly satisfying. Indeed, TD-DFT reproduces the gap between the two peaks (32 nm vs. 37 nm), their relative intensities (0.44 vs. 0.46), as well as the bathochromic shift with respect to **2b** (56 nm vs. 64 nm). The 356 nm (324 nm) absorption mainly corresponds to a HOMO to LUMO (HOMO to LUMO+1) transition with a smaller HOMO−1 to LUMO+1 (HOMO−1 to LUMO) contribution. These orbitals, sketched in Figure 5, are basically completely delocalized and no

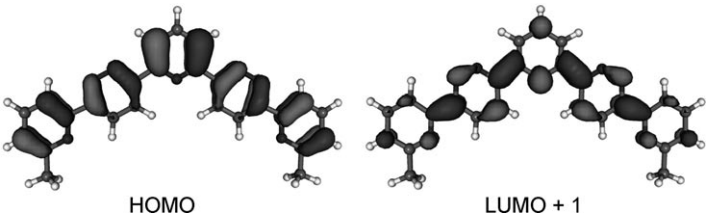

Figure 4. Relevant molecular orbitals for **2b**, computed at the PCM-(CH_2Cl_2)-CAM-B3LYP/6-311+G(2d,p) level and plotted with a contour threshold of 0.30 a.u.

Table 4. Photophysical properties of dipyrroles **1b** and **1c** and dipyridazines **2b** and **2c** in methanol and dichloromethane.

Entry	Solvent	Ligand	λ_{abs} [nm]	ε [$mol^{-1}Lcm^{-1}$]	$\tilde{\nu}_{exc}$[a] [cm^{-1}]	$\tilde{\nu}_{exc}$[a] [cm^{-1}]	ϕ_f[b,c]
1	CH_2Cl_2	**2b**	316	38000			
			257	23800			
2		**2c**	318	44600			
			260	28600			
3		**1b**	380	25900	26500	24250	0.12
			343	56300			
4		**1c**	380	26900	26500	24200	0.15
			341	58600			
5	MeOH	**1b**	378	29500	26600	23600	0.01
			341	62100			
6		**1c**	378	29400	26600	23300	0.01
			340	64200			

[a] Accuracy ±50 cm^{-1}. [b] Fluorescence quantum yields were calculated relative to quinine sulfate in 0.5 M H_2SO_4 solution.[24] [c] Measured error is ±10%.

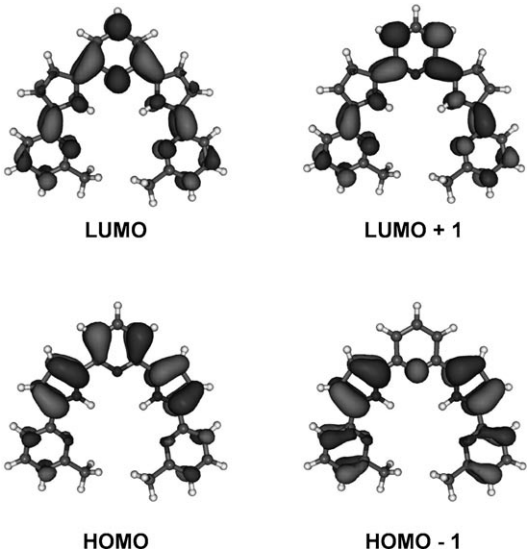

Figure 5. Relevant molecular orbitals for **1b** in its optimal geometry, computed at the PCM-(CH_2Cl_2)-CAM-B3LYP/6-311+G(2d,p) level and plotted with a contour threshold of 0.30 a.u.

strong electronic transfer is associated with the two absorption bands, though the HOMO−1 to LUMO+1 component implies a displacement of charge from the terminal pyridine rings to the central one. For the record, we also computed the spectra for C_{2v} geometries with or without a central water molecule (analogous to the crystal structure, see below), and it can be seen in Figure 3C that all structures show very similar absorption patterns. The small impact of the central water molecule may be ascribed to the π symmetry of the relevant orbitals: they are almost unaffected by H-bonds between water and the lone pairs of the pyridine rings.

Changing the concentration of dipyridazines **2b** and **2c**, and dipyrroles **1b** and **1c**, does not modify their absorption features in CH_2Cl_2 (data not shown). Moreover, the absorption peaks in both pyridazine and pyrrole series express a large molar extinction coefficient on the order of $\varepsilon \approx 10^4\ mol^{-1}\,L\,cm^{-1}$ for the two series (Table 4).

The absorption characteristics of dipyrroles were also investigated in MeOH, while dipyridazines **2b** and **2c** remain insoluble in the protic solvents. The absorptions of dipyrroles **1b** and **1c** in MeOH show similar profiles to those in CH_2Cl_2 and again are not concentration-dependent (Figure 3B). This observation indicates that MeOH does not induce formation of aggregates of the pyrrole species at the tested concentrations (10^{-4}–$10^{-5}\ mol\,L^{-1}$). The absence of a solvatochromism may result from the constrained conformation of tripyridyl–dipyrrolic ligands **1b** and **1c** trapping a molecule of water, which probably restricts interactions with protic solvents.

The fluorescence characteristics of **1b** and **1c** were also examined in both protic and aprotic solvents (MeOH and CH_2Cl_2), whereas dipyridazines **2b** and **2c** do not fluoresce in CH_2Cl_2. The excitation and emission fluorescence spectra, the positions of the excitation and emission fluorescence maxima and the quantum yields are presented in Figure 6 and Table 4. The excitation spectra (Figure 6A for CH_2Cl_2 and B for MeOH), measured in the region of 40000–24000 cm^{-1}, coincide with the absorption spectra within experimental error, that is, the entire emission results from a common Franck–Condon excited state in each case. The fluorescence emission behavior of compounds **1b** and **1c** (Table 4, $\tilde{\nu}_{em} \approx 2\times10^4\ cm^{-1}$ in MeOH and CH_2Cl_2) is independent of the excitation wavelength in both solvents (data not shown), which indicates adherence to Kasha's rule.[25] In CH_2Cl_2, both pyrrole derivatives reveal similar high emission yields (Table 4; $\phi_f = 0.15$ and 0.12 for **1b** and **1c**, respectively), but ten times higher than in MeOH (Table 4; $\phi_f \approx 0.01$ for **1b** and **1c**). Indeed, the effect of solvent on the de-excitation mode of the pyrrole units could be analyzed to rationalize the quantum yield in MeOH. As observed by MacManus-Spencer et al. in 2-(2′-pyridyl)pyrrole structures,[6b] the absence of a red-shifted emission band, which is one hallmark of an excited-state double proton-transfer process, was also found in the emission spectra of dipyrroles **1b** and **1c** in MeOH.

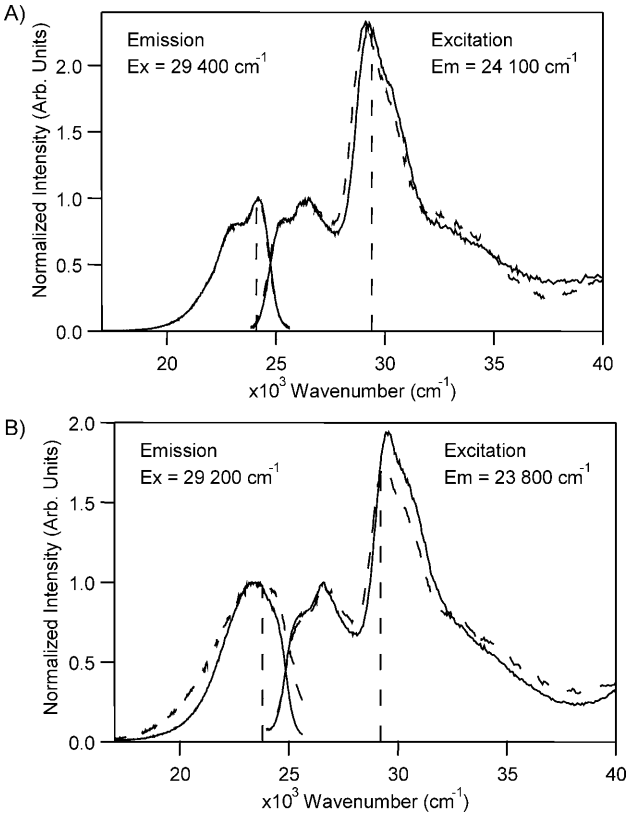

Figure 6. A) Excitation (measured at 24100 cm^{-1}) and emission (excited at 29400 cm^{-1}) spectra of **1b** (– – –) and **1c** (——) in dichloromethane. All spectra are normalized to the maximum intensity. B) Excitation (measured at 23800 cm^{-1}) and emission (excited at 29200 cm^{-1}) spectra of dipyrroles **1b** (– – –) and **1c** (——) in methanol.

Solid-state structures: Single-crystal X-ray diffraction analysis of tripyridyl–dipyrroles **1b** and **1c** were undertaken to establish their molecular geometries and intermolecular interactions in the solid state, in anticipation of a potential ability to embed a metal ion. ^{1}H NMR analysis of **1b** and **1c** predicted organization of averaged symmetrical structures supporting the modelling calculations. For example, the terminal methyl proton signals are observed as one singlet (δ = 2.64 ppm) for **1b** and two singlets (δ = 2.33 and 2.61 ppm) for **1c**. The free dipyrrole ligands crystallized from dried, distilled hexane/chloroform (4:1), and both have a coordinated water molecule (Figure 7).

The structures reveal a bent and almost flat conformation similar to the calculated structures. Thus, both molecules **1a** and **1b** have all five pyridyl and pyrrolyl ring endocyclic nitrogen atoms oriented towards the cavity and all aryl–aryl linkages in *cis* conformation, which is reinforced by intermolecular H-bonds between NH_{pyr} and O_{water} of the two pyrrole units and N_{pyd} and H_{water} of the two terminal pyridine moieties (selected bond lengths, distances and angles are given in Table 5). These H-bonds are both 2.17 Å in length for **1b**, and a weak twist of the conformation is observed between the pyrrole and the terminal pyridine planes with an angle

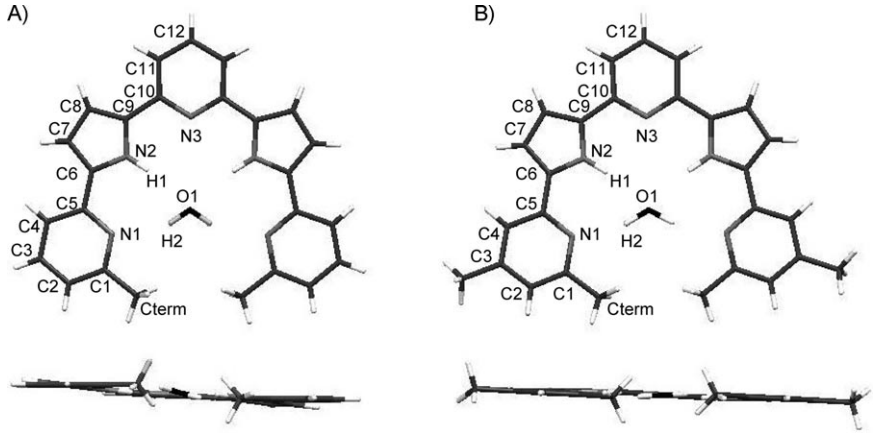

Figure 7. Mercury diagrams of dipyrroles **1b** (A) and **1c** (B) determined by X-ray diffraction.

Table 5. Selected bond lengths [Å], distances [Å], and bond angles [°] for dipyrrole compounds **1b** and **1c** and for the dipyrrole dimetal complex of **1b** with copper(II).

	1b (X = O)	**1c** (X = O)	**1b-Cu$_2$** (X = Cu)
N1−H2	2.17(5)	2.02(4)	–
N1−N1	5.653(4)	5.604(3)	6.53(1)
N1−N2	2.859(3)	2.852(2)	2.69(1)
N1−N3	5.133(4)	5.120(3)	5.21(1)
N1−X1	2.962(3)	2.936(2	2.024(9)
N2−N2	4.639(4)	4.632(7)	5.04(1)
N2−N3	2.747(3)	2.748(2)	2.92(1)
N2−X1	3.015(3)	3.021(2)	2.01(1)
N3−X1	3.398(5)	3.415(3)	3.53(1)
N3−H2	3.94(5)	3.96(4)	–
X1−H1	2.167(3)	2.112(2)	–
X1−X1	–	–	3.082(2)
X1−Cl1	–	–	2.526(3)
X1−O1	–	–	1.930(6)
X1−O2	–	–	2.00(1)
C1−C2	1.388(5)	1.381(3)	1.42(2)
C2−C3	1.378(5)	1.381(3)	1.34(2)
C3−C4	1.368(5)	1.372(3)	1.39(2)
C4−C5	1.396(4)	1.391(3)	1.39(1)
C5−C6	1.450(4)	1.459(3)	1.46(2)
C6−C7	1.388(4)	1.378(3)	1.45(2)
C7−C8	1.396(5)	1.399(3)	1.43(2)
C8−C9	1.383(4)	1.374(3)	1.42(2)
C9−C10	1.463(4)	1.456(3)	1.50(2)
C10−C11	1.377(4)	1.393(3)	1.36(2)
C11−C12	1.376(4)	1.373(3)	1.38(2)
C_{term}···C_{term}	3.825(5)	3.772(4)	4.79(2)
N1-N2-N3	132.6(1)	132.23(9)	136.4(5)
N2-N3-N2	115.2(2)	115.00(9)	119.2(6)
N1-X1-N2	–	–	83.7(4)
X1-Cl1-X1	–	–	75.2(1)
X1-O1-X1	–	–	106.0(5)

of 6.1°. The molecule of water positioned in the centre of the bent conformation deviates from the plane of the central pyridine ring by 11.4°, while the two external pyridine rings are almost mutually coplanar. Thanks to the electron-donating effect of an additional *para* methyl group on each terminal pyridine rings, the H-bond distances vary slightly in **1c** (NH_{pyr}···O_{water} 2.112 Å and N_{pyd}···H_{water} 2.02 Å). The methyl groups of **1c** are closer together than those of **1b** (C_{term}···C_{term} 3.772 and 3.825 Å respectively), while the planar conformation of **1c** is maintained (C6-N2-$C9_{pyr}$/C1-N1-$C5_{term\ pyd}$ 1.8°). However, the distance between the terminal methyl groups does not undercut the sum of the van der Waals distances, in confirmation of the strained situation of a square-planar block conformation.

The dipyrrolic ligands **1** are arranged in pseudo-helical pillars composed of alternating opposite orientations of the monomers (Figure 8A), propagation of which along the crystallographic *b* axis leads to a solvent channel (Figure 8B).

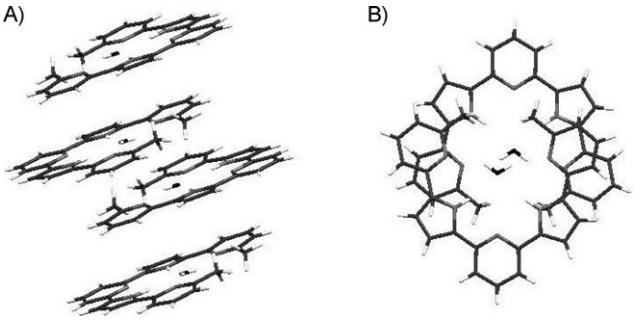

Figure 8. Mercury diagrams of the dipyrrole–dipyrroles **1b** arrangement (identical to **1c**, see Supporting Information)

Gas-phase geometry of **1b** was optimized at the PBE0/6-311G(d,p) level with and without a central water molecule. For the latter structure, the theory/experiment discrepancies are relatively small, though the water molecule is not located in a perfectly symmetric position as in the solid state. The performance of PBE0 is illustrated by the relatively accurate estimates for the challenging non-covalent distances, for example, C_{term}···C_{term} 3.735 Å (2% error), N1−N1 5.481 Å (3% error) and N2−N2 4.547 Å (2% error). For the position of the central water molecule, DFT yields an N3−O1 distance of 3.490 Å (3% error) and an average H1−O1 separation of 2.067 Å (5% error). For the N1-N2-N2-N1 dihedral angle, theory (10.9°) and experiment (2.9°) provide diverging estimates, an expected outcome for a parameter more sensitive to solid-state packing effects. When the central water molecule is removed, the predicted twist of the structure strongly increases with a C_{term}···C_{term} distance of 4.249 Å and an N1-N2-N2-N1 dihedral angle of 24.2°; in other words, the complexed molecule tends toward a flattened structure, which hints that water has a large impact on the measured geometrical parameters. From an energetic

point of view, the deformation of **1b** induced by the central water molecule is estimated at 2.7 kcal mol^{-1}, whereas the energy inside the dipyrrole units has been evaluated to be 10.9 kcal mol^{-1}. This relatively large stabilization energy is consistent with the nearly optimal position of the water molecule, which interacts with **1b** through several H-bonds.

The potential for coordination and molecular distortion of the tripyridinyl–dipyrrole ligands was addressed by studying a copper(II) salt. The prediction was confirmed by the X-ray analysis of a crystal complex of ligand **1b** that formed successfully in the presence of $Cu^{II}(OAc)_2$ in methanol/dichloromethane solution (Figure 9). Two copper atoms are trapped by one pentadentate single ligand **1b** in the bifurcated chloro-, acetato-, and methoxyl-bridged 1:2 dicopper(II) complex **1b-Cu$_2^{II}$**. Both copper(II) atoms are pentacoordinate in a distorted square. Each square involves two nitrogen atoms, one from a deprotonated pyrrole moiety ($d_{N2-Cu1}=2.01$ Å) and the other from a peripheral pyridine residue ($d_{N1-Cu1}=1.996$ Å), while the nitrogen atom of the central pyridine ring remains too remote to interact ($d_{N3-Cu1}=3.53$ Å). To allow the two copper centres to embed in the ligand cavity, the ligand is slightly distorted from its otherwise planar conformation (central pyridine vs. pyrrole 6.6°; pyrrole vs. terminal pyridine 7.5° and central pyridine vs. terminal pyridine 13.5°; for **1b**: 2.7, 6.1 and 2.3°, respectively). The N_{pyr}-Cu^{II}-$N_{term\ pyd}$ and $N_{term\ pyd}$-N_{pyr}-$N_{central\ pyd}$ bond angles are about 83.7 and 136.4°, respectively. Consequently, the pyridine–pyrrole–pyridine linkages end up twisted, while all nitrogen atoms of the pentadentate ligand remain pointed towards the inner copper atoms in a concave deformation. This result suggests that the ligand can adapt to various sizes of metal ions with a variation of ±0.846 Å between the nitrogen atoms of terminal pyridine units ($d_{N1-N1}=5.653$ Å for **1b** and 6.53 Å for **1b-Cu$_2^{II}$**) and over ±0.97 Å between the two end methyl groups ($d_{Cterm\cdots Cterm}=3.825$ Å for **1b** and $d_{Cterm\cdots Cterm}=4.79$ Å for **1b-Cu$_2^{II}$**]. The two copper(II) ions are located only 3.082 Å from each other. More interestingly, to accommodate the two transition-metal ions, the coordination preserves a single bridging acetate ion and association with a molecule of methanol and a chloride ion, which bridge the two copper(II) cations with Cu1-O1-Cu1 and Cu1-Cl1-Cu1 angles of 106.0 and 75.2°, respectively. Both the methanol molecule and chloride anion, originating from the solvents, replaced the acetate counterions of the two copper ions with distances ($d_{Cu1-O1}=1.930$, $d_{Cu1-Cl1}=2.526$ Å) similar to those found in other choride-bridged copper structures. The chloride ion is oriented toward the inside cavity of the dinuclear complex while the acetate and methanol ligands point to the convex side.

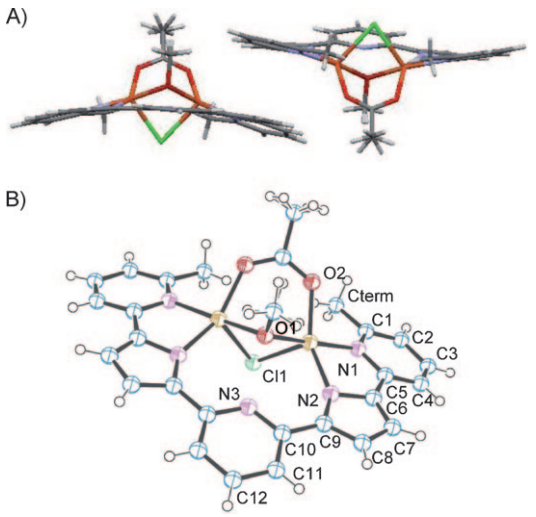

Figure 9. A) Mercury diagrams of Cu^{II} complex **1b-Cu$_2^{II}$**. B) ORTEP of dimetallic complex **1b-Cu$_2^{II}$**, determined by X-ray diffraction.

Conclusion

The synthesis and characterisation of two chromophore strands in which two electron-rich pyrrole units (donors) are sandwiched between pyridine cores (acceptors) was achieved. A smooth, green electrosynthetic approach to alternating pyrrolic–pyridine sequences has been designed. This strategy required access to alternating tripyridyl–dipyridazine precursors in sufficient quantities to investigate their electrochemical ring-contraction behavior, which was provided by a Negishi metal cross-coupling methodology involving 2-pyridyl zinc bromide reagents **12a–c** and 2,6-bis-(6-trifluoromethanesulfonylpyridazin-3-yl)pyridine **14**. This procedure provided the desired tripyridyl–dipyridazines **2a–c** in reproducible yields, which increased further in the presence of methyl groups on the metallated halogenopyridine (30–95%). Preparative electrochemical reduction of tripyridyl–dipyridazines **2b** and **2c** in THF/acetate buffer/acetonitrile gave target tripyridyl–dipyrroles **1b** and **1c** in good yields of 71 and 93%, respectively. The highly fluorescent properties of donor–acceptor tripyridyl–dipyrrole ligands **1b** and **1c** were determined ($\tilde{\nu}_{em}\approx 2\times10^4$ cm^{-1} in MeOH and CH_2Cl_2), and both exhibit a remarkable quantum yield in CH_2Cl_2 ($\phi_f=0.15$ and 0.12 for **1b** and **1c**, respectively), which drastically dropped in MeOH ($\phi_f\approx0.01$).

From a structural point of view, the X-ray diffraction analyses of the tripyridyl-dipyrrole sequences in **1b** and **1c** reflect the all-*cis* conformation in the solid state predicted by quantum chemical calculations.[22] Additionally, the donor–acceptor ligands encapsulate a molecule of water, which contributes to the energetic stability of their planar organisation and may further restrict the rotational freedom, which generally strongly depends on the extent heterocycle linkage. Theoretical calculations fully complement and support the explanations for the experimental observations, by providing a complexation energy exceeding 10 kcal mol^{-1} for the central water molecule. The ability of tripyridyl–dipyrrole ligand **1b** to complex with a metal cation was explored. In the presence of a copper(II) salt, a bifurcated 1:2 complex in which two copper atoms are trapped by a single

polydentate ligand was isolated in the solid state. The two copper(II) ions are pentacoordinate in a distorted square involving four nitrogen atoms from both deprotonated pyrrole rings and the two external pyridine residues. Comparative X-ray analysis of the ligand **1b** and complex **1b-Cu_2^{II}** emphasizes the degree of molecular distortion displayed by such molecular strands and suggests that versatile formation of complexes with other geometries may be achieved. This result sheds light on the structure/property relationship of the tripyridyl–dipyrrole ligands and provides important information for future design of complex-based devices exploiting the high cooperativity potential in dimetallic binding. Thus, these donor–acceptor pyrrole strands are of interest for the preparation of new bifunctional complexes including those with anions or H-bonding with organic bases. Indeed, alternating dipyrrole ligands are expected to be able to participate further in the self-assembly of supramolecular architectures through intermolecular bonds mediated by metal atoms replacing the central water molecule. Current work aims at investigating metal-binding properties of such original donor–acceptor ligands with lanthanides. They also may be valuable models for study of steric and electronic effects on associative biological interactions or other H-bonded molecules. Preliminary in vitro studies were performed to determine whether the new set of pyridazine and pyrrole derivatives described above can induce cytotoxicity and/or bioactive effects in living cells from different tissular origins. Assays were performed by monitoring cell viability and growth activity of six different tumour cell lines representative of the most frequent solid tumours in humans (liver, colon, prostate, breast and lung) and one normal diploid skin fibroblastic cell line, exposed to increasing concentrations of the compounds (from 0.1 to 25 μM) for 1 and 2 d. Table 6, which lists data for representative compounds, highlights that pyridazines **2a** and **2b** and pyrrole derivatives **1b** and **1c** can penetrate cell membranes, and pyrrolic derivative seem to be effective in inducing cytotoxicity.

Table 6. Antiproliferative cell activity [μM].

Molecule	Huh7[a]	Caco2[b]	PC3[c]	MDA-MB231[d]	NCI[e]	Fibroblasts[f]
2a	15	3	25	4	25	>25
2b	7	7	5	4	15	10
2c	>25	>25	>25	>25	>25	>25
1b	1.2	3	3	3	8	5
1c	2.5	2	3	5	7	10

[a] Huh7: liver. [b] Caco2: colon. [c] PC3: prostate. [d] MDA-MB231: breast. [e] NCI: lung. [f] Fibroblasts: reference.

The obvious advantages of the developed one-pot electrosynthetic strategy starting from more easily accessible pyridazine precursors, make our approach attractive for preparing a number of otherwise inaccessible functionalized molecular strands in which several pyrrole units are linked by various heterocyclic spacers. Elaboration of such polyfunctional metal complexes is currently in progress.

Experimental Section

General procedure for the synthesis of 6-tributylstannylpyridines 11a,[26] 11b[26,27] and 11c: *n*BuLi (2.5 mol L^{-1} in hexanes, 1 equiv) was added to a solution of 2-bromopyridine (1 equiv) in THF (2 mL $mmol^{-1}$) at −78 °C. After 30 min, tributylstannyl chloride (1 equiv) was added to the resulting dark red solution. Then the solution was stirred for 1 h at −78 °C and an additional 1 h at room temperature. The reaction mixture was quenched with saturated aqueous NH_4Cl solution. The aqueous phase was extracted with Et_2O, and the organic layer washed with brine, dried over $MgSO_4$ and concentrated to dryness. After purification by distillation under reduced pressure with a Kugelrohr apparatus, the compounds were obtained as pale yellow oils.

2,4-Dimethyl-6-(tributylstannyl)pyridine (11c): Following the general procedure, a solution of 2-bromo-4,6-dimethylpyridine (2.0 g, 10.75 mmol), *n*BuLi (2.5 mol L^{-1} in hexanes, 4.3 mL, 10.75 mmol) and tributylstannyl chloride (2.9 mL, 10.75 mmol) in THF (20 mL) was stirred at −78 °C for 1 h and an additional 1 h at room temperature. Distillation of the crude product (218 °C, 1.1 mbar) obtained after work-up yielded 3.7 g (86%, overestimated yield due to remaining trace of stannyl reagent) of **11c** as a pale yellow oil. ^{1}H NMR (300 MHz, $CDCl_3$, 25 °C): δ = 7.03 (s, 1H), 6.81 (s, 1H 2.51 (s, 3H), 2.25 (s, 3H), 1.69–1.53 (m, 6H), 1.41–1.29 (m, 6H), 1.14–1.08 (m, 6H), 0.97–0.88 ppm (m, 9H); ^{13}C NMR (75.5 MHz, $CDCl_3$, 25 °C): δ = 172.5, 158.6, 144.1, 130.8, 122.9, 29.4, 25.0, 21.1, 17.8, 14.0, 10.1 ppm; MS (70 eV): *m/z* (%): 396 (2) $[M]^+$, 339 (100) $[M-Bu]^+$; HRMS: *m/z* calcd for $[M+H]^+$ ($C_{19}H_{36}N^{116}Sn$): 394.1886; found 394.1866.

6,6′-(Pyridine-2,6-diyl)dipyridazin-3(2*H*)-one (17): Glyoxylic acid (2.3 g, 30.67 mmol) was added to a solution of K_2CO_3 (6.8 g, 49.43 mmol) in water (40 mL) at 0 °C. After homogenisation, 2,6-diacetylpyridine **15** (2.0 g, 12.26 mmol) was added and the mixture was stirred at 50 °C until total dissolution of the compounds. After cooling at 0 °C, glacial acetic acid (10 mL) and then monohydrate hydrazine (5 mL) were added dropwise. After 2 h at reflux, the reaction mixture was cooled to 0 °C and neutralized with K_2CO_3 (powder then saturated aqueous solution). The resulting precipitate was filtered, washed distilled water and 2-propanol. Desired compound **17** in a mixture with its tautomer (3.0 g, 91%) was obtained as a pale yellow powder. M.p. 284 °C; ^{1}H NMR (300 MHz, [D$_6$]DMSO, 25 °C): δ = 13.13 (brs, 2H), 8.52 (d, *J* = 9.9 Hz, 2H), 8.11–8.04 (m, 3H), 7.05 ppm (d, *J* = 9.9 Hz, 2H), due to the existence of its tautomer (ca. 5%) most of the signals appear twice; ^{13}C NMR (75 MHz, [D$_6$]DMSO, 25 °C): δ = 160.7, 151.3, 143.1, 138.8, 131.0, 130.0, 119.4 ppm; MS (70 eV): *m/z* (%): 267 (100) $[M]^+$, 238 (6) $[M-N_2]^+$, 211 (32) $[M-2N_2]^+$.

2,6-Bis(6-chloropyridazin-3-yl)pyridine (13): A solution of dipyridazinone **17** (1.9 g, 6.25 mmol) in $POCl_3$ (15 mL) was heated to reflux for 18 h. After cooling, the reaction mixture was distilled under reduced pressure to remove excess $POCl_3$. Then the residue was carefully hydrolyzed by addition of iced water and neutralized with 1 mol L^{-1} aqueous NaOH solution. The aqueous layer was extracted with CH_2Cl_2. The combined organic layers were dried (Na_2SO_4) and concentrated. Flash chromatography on silica gel (AcOEt) gave pure compound **13** (1.1 g, 60%) as a pale yellow powder. M.p. >230 °C; ^{1}H NMR (300 MHz, $CDCl_3$, 25 °C): δ = 8.77 (d, *J* = 7.9 Hz, 2H), 8.62 (d, *J* = 9.0 Hz, 2H), 8.10 (t, *J* = 7.9 Hz, 1H), 7.67 ppm (d, *J* = 9.0 Hz, 2H); ^{13}C NMR (75 MHz, $CDCl_3$, 25 °C): δ = 157.4, 157.2, 152.3, 138.8, 128.7, 126.7, 123.0 ppm; MS (70 eV): *m/z* (%): 304 (17) $[M]^+$, 240 (100) $[M-Cl-N_2]^+$, 205 (9) $[M-2Cl-N_2)]^+$; HRMS: *m/z* calcd for $[M+Na]^+$ ($C_{13}H_7Cl_2N_5Na$): 325.9976; found 325.9950.

2,6-Bis(6-trifluoromethanesulfonylpyridazin-3-yl)pyridine (14): Triflic anhydride (1.9 mL, 11.22 mmol)was added to a cooled (0 °C) solution of **17** (1.0 g, 3.74 mmol) and 4-dimethylaminopyridine (23 mg, 0.19 mmol) in pyridine (5 mL). The reaction mixture was allowed to warm to room temperature over 6 h. Water (30 mL) was added and the mixture was extracted with CH_2Cl_2 (4×10 mL). The combined organic layers were washed with brine (30 mL), dried (Na_2SO_4) and concentrated to dryness. Chromatography on silica gel (petroleum ether/CH_2Cl_2/Et_2O, gradient from 100:0:0 to 70:20:10) afforded **14** (1.36 g, 69%) as brown powder. M.p.: 143 °C; ^{1}H NMR (300 MHz, [D$_6$]DMSO, 25 °C): δ = 9.24 (d, *J* = 9.2 Hz,

2H), 8.74 (d, $J=7.9$ Hz, 2H), 8.34 (t, $J=7.9$ Hz, 1H), 8.31 ppm (d, $J=9.2$ Hz, 2H); ^{13}C NMR (75.5 MHz, [D$_6$]DMSO, 25°C): $\delta=160.8$, 159.3, 151.6, 139.9, 131.4, 123.2, 122.7, 120.3 ppm; MS (70 eV): *m/z* (%): 531 (48) $[M]^+$, 370 (51) $[M-SO_2CF_3-N_2]^+$, 342 (100) $[M-SO_2CF_3-2N_2]^+$; HRMS: *m/z* calcd for $[M+Na]^+$ ($C_{15}H_7F_6N_5NaO_6S_2$): 553.9634; found: 553.9628.

General procedure for synthesis of dipyridazines 2a, 2b and 2c by Negishi coupling reaction: A solution of the requisite bromopyridine (1.6 equiv) in THF (3 mL mmol^{-1} of bromopyridine) at −78°C was treated with *n*BuLi (2.5 mol L^{-1} in hexanes, 1.6 equiv). The mixture was stirred for 30 min, and then a solution of zinc chloride (0.7 mol L^{-1} in THF, 1.6 equiv) was added by canula at −78°C. At the end of the addition, the mixture was allowed to warm to room temperature and stirred for 30 min. Then a solution of tetrakis(triphenylphosphine)palladium (0.05 equiv) and activated dipyridazine **14** (1.0 equiv) in THF (6 mL mmol^{-1} of bromopyridine) was added by a canula at this temperature. After 48 h at reflux, the mixture was quenched with saturated aqueous $NaHCO_3$ (30 mL) and 25 mol L^{-1} aqueous NH_4OH (50 mL) solutions, and the resulting solution was stirred for 24 h. The heterogeneous mixture was filtered through a pad of Celite, which was washed with CH_2Cl_2 then with 25 mol L^{-1} aqueous NH_4OH. The filtrate was extracted with CH_2Cl_2 (3×50 mL). The combined organic layers were dried over Na_2SO_4 and the solvents were removed in vacuo to afford the respective reaction product, which was purified by flash chromatography on silica gel or crystallization.

2,6-Bis[6-(pyridin-2-yl)pyridazin-3-yl]pyridine (2a): Following the general procedure, a solution of activated dipyridazine–pyridine **14** (1.06 g, 2.0 mmol) and tetrakis(triphenylphosphine)palladium (0.46 g, 0.32 mmol) in THF (40 mL) was added to the organozinc reagent [prepared from 2-bromopyridine (1.01 g, 6.4 mmol), *n*Buli (2.4 M in hexanes, 3.0 mL, 7.0 mmol) in THF (20 mL)] and zinc chloride (0.7 mol L^{-1} in THF, 10.0 mL, 7.0 mmol). The reaction mixture was stirred at reflux for 48 h. Crystallization (AcOEt) of the crude product obtained by following the general work-up procedure yielded 210 mg (27%) of pure **2a** as a pale yellow solid. M.p. 258°C; ^{1}H NMR (300 MHz, $CDCl_3$, 25°C): $\delta=8.87$–8.71 (m, 10H), 8.10 (t, $J=8.1$ Hz, 1H), 7.89 (dt, $J=7.8$, 1.8 Hz, 2H), 7.41 ppm (ddd, $J=7.5$, 4.8, 1.2 Hz, 2H); ^{13}C NMR (75 MHz, $CDCl_3$, 25°C): $\delta=158.3$, 157.8, 153.3, 153.1, 149.4, 138.5, 137.2, 128.5, 125.1, 124.8, 122.6, 121.7 ppm; UV/Vis (CH_2Cl_2): $\lambda(\varepsilon)=315$ (38200), 290 (33600), 256 nm (29250 mol^{-1} dm^3 cm^{-1}); MS (70 eV): *m/z* (%): 389 (46) $[M]^+$, 361 (64) $[M-N_2]^+$, 128 (100) $[PyrC_4H_2]^+$; HRMS: *m/z* calcd for $[M+H]^+$ ($C_{23}H_{16}N_7$): 390.1473; found 390.1467.

2,6-Bis[6-(6-methylpyridin-2-yl)pyridazin-3-yl]pyridine (2b): Following the general procedure, a solution of activated dipyridazine–pyridine **14** (532 mg, 1.00 mmol) and tetrakis(triphenylphosphine)palladium (231 mg, 0.20 mmol) in THF (20 mL) was added to the organozinc reagent [prepared from 2-bromo-6-methylpyridine (550 mg, 3.20 mmol) and *n*Buli (2.5 mol L^{-1} in hexanes, 1.4 mL, 3.50 mmol) in THF (10 mL)] and zinc chloride (0.7 M in THF, 5.0 mL, 3.50 mmol). The reaction mixture was stirred at reflux for 48 h. Chromatography on silica gel (CH_2Cl_2/Et_2O, gradient from 100:0 to 50:50) of the crude product obtained by following the general work-up procedure yielded 284 mg (68%) of pure **2b** as a white solid. M.p. 259°C; ^{1}H NMR (300 MHz, $CDCl_3$, 25°C): $\delta=8.88$ (d, $J=7.9$ Hz, 2H), 8.81 and 8.78 (AB Syst, $J=8.9$ Hz, 4H), 8.57 (d, $J=7.8$ Hz, 2H), 8.12 (t, $J=7.9$ Hz, 1H), 7.80 (t, $J=7.8$ Hz, 2H), 7.28 (d, $J=7.8$ Hz, 2H), 2.68 ppm (s, 6H); ^{13}C NMR (75 MHz, $CDCl_3$, 25°C): $\delta=158.6$, 158.3, 157.8, 153.2, 152.7, 138.4, 137.3, 125.1, 124.9, 124.3, 122.5, 118.7, 24.6 ppm; UV/Vis (CH_2Cl_2): $\lambda(\varepsilon)=316$ (38000), 257 nm (23800 mol^{-1} dm^3 cm^{-1}); MS (70 eV): *m/z* (%): 417 (100) $[M]^+$, 389 (94) $[M-N_2]^+$; HRMS: *m/z* calcd for $[M+Na]^+$ ($C_{25}H_{19}N_7Na$): 440.1600, found 440.1599.

2,6-Bis[6-(4,6-dimethylpyridin-2-yl)pyridazin-3-yl]pyridine (2c): Following the general procedure, a solution of activated dipyridazine–pyridine **14** (385 mg, 0.72 mmol) and tetrakis(triphenylphosphine)palladium (167 mg, 0.14 mmol) in THF (20 mL) was added to the organozinc reagent [prepared from 2-bromo-4,6-dimethylpyridine (431 mg, 2.32 mmol) and *n*Buli (2.5 mol L^{-1} in hexanes, 1.0 mL, 2.54 mmol) in THF (10 mL)] and zinc chloride (0.7 M in THF, 3.6 mL, 2.54 mmol). The reaction mixture was stirred at reflux for 48 h. Chromatography on silica gel (CH_2Cl_2/Et_2O, gradient from 100:0 to 50:50) of the crude product obtained by following the general work-up procedure yielded 306 mg (95%) of pure **2c** as a pale yellow solid. M.p.: 269°C; ^{1}H NMR (300 MHz, $CDCl_3$, 25°C): $\delta=8.86$ (d, $J=7.8$ Hz, 2H), 8.77 and 8.75 (AB system, $J=8.9$ Hz, 4H), 8.42 (s, 2H), 8.10 (t, $J=7.8$ Hz, 1H), 7.10 (s, 2H), 2.63 (s, 6H), 2.44 ppm (s, 6H); ^{13}C NMR (75.5 MHz, $CDCl_3$, 25°C): $\delta=158.5$, 158.1, 157.7, 153.2, 152.4, 148.6, 138.4, 125.4, 125.3, 124.9, 122.5, 119.9, 24.3, 21.1 ppm; UV/Vis (CH_2Cl_2): $\lambda(\varepsilon)=318$ (44600 mol^{-1} m^3 cm^{-1}), 260 nm (28600 mol^{-1} dm^3 cm^{-1}); MS (70 eV): *m/z*: 445 (36) $[M]^+$, 417 (33) $[M-N_2]^+$; HRMS: *m/z* calcd for $C_{27}H_{23}N_7$: 445.2015; found: 445.2016.

General procedure for the synthesis of dipyrroles 1b and 1c by electrochemical ring contraction: Dipyridazine **2b** or **2c** (70 to 200 mg) was dissolved in THF/acetate buffer/CH_3CN (5:4:1, 90 mL), and the solution introduced into the cathodic compartment of the electrochemical cell. The same solvent was put in the anodic compartment. Prior to and during electrolysis at E_w, the catholyte was deaerated with argon and stirred magnetically. The course of the reaction was followed by cyclic voltammetry in the cathodic compartment, and the electrolysis was stopped when the consumption of the starting substrate was complete (8 F mol^{-1}). Then the solvents were partially evaporated and the resulting precipitate was collected by filtration. The yellow solid was dissolved in CH_2Cl_2 and washed with saturated aqueous $NaHCO_3$ solution and water. The organic layer was dried (Na_2SO_4) and concentrated to dryness. After purification by crystallisation (hexane/chloroform 4:1), dipyrroles **1b** and **1c** were obtained as yellow powders.

2,6-Bis[5-(6-methylpyridin-2-yl)pyrrol-2(1*H*)-yl]pyridine (1b): A solution of dipyridazine **2b** (150 mg, 0.36 mmol) in THF/acetate buffer/CH_3CN (5:4:1, (100 mL) was reduced at $E_w=-1.25$ V/SCE. Then crystallization (hexane/chloroform 4:1) of the crude product, obtained by following the general work-up procedure, yielded pure **1b** (101 mg, 71%) as a yellow powder. M.p. 103°C; ^{1}H NMR (300 MHz, $CDCl_3$, 25°C): $\delta=11.50$ (br s, 2H), 7.60 (t, $J=7.8$ Hz, 2H), 7.56 (t, $J=7.5$ Hz, 2H), 7.49 (d, $J=7.5$ Hz, 2H), 7.35 (d, $J=7.8$ Hz, 1H), 6.94 (d, $J=7.5$ Hz, 2H), 6.82–6.76 (m, 4H), 2.66 ppm (s, 6H); ^{13}C NMR (75 MHz, $CDCl_3$, 25°C): $\delta=157.4$, 150.3, 149.6, 137.0, 136.9, 134.2, 133.0, 120.4, 116.7, 115.5, 110.2, 108.8, 24.7 ppm; UV/Vis (CH_2Cl_2): $\lambda(\varepsilon)=380$ (25900), 343 nm (56300 mol^{-1} dm^3 cm^{-1}); UV/Vis (MeOH): $\lambda(\varepsilon)=378$ (29500), 341 nm (62100 mol^{-1} dm^3 cm^{-1}); MS (70 eV): *m/z* (%): 392.1 (100) $[M+H]^+$; HRMS: *m/z* calcd for $[M+H]^+$ ($C_{25}H_{22}N_5$): 392.1875; found 392.1869.

2,6-Bis[5-(4,6-dimethylpyridin-2-yl)pyrrol-2(1*H*)-yl]pyridine (1c): A solution of dipyridazine **2c** (71 mg, 0.16 mmol) in THF/acetate buffer/CH_3CN (5:4:1, 100 mL) was reduced at $E_w=-1.20$ V/SCE. Then crystallisation (hexane/chloroform 4:1) of the crude product, obtained by following the general work-up procedure, yielded pure **1c** (62 mg, 93%) as a yellow powder. M.p. 219°C; ^{1}H NMR (300 MHz, $CDCl_3$, 25°C): $\delta=11.50$ (br s, 2H), 7.58 (t, $J=7.8$ Hz, 1H), 7.35 (d, $J=7.8$ Hz, 2H), 7.32 (s, 2H), 6.78–6.75 (m, 6H), 2.61 (s, 6H), 2.33 ppm (s, 6H); ^{13}C NMR (75.5 MHz, $CDCl_3$, 25°C): $\delta=157.0$, 150.1, 149.6, 147.9, 136.8, 134.0, 133.0, 121.6, 117.4, 115.3, 109.9, 108.7, 24.4, 21.1 ppm; UV/Vis (CH_2Cl_2): $\lambda(\varepsilon)=380$ nm (26900 mol^{-1} m^3 cm^{-1}), 341 (58600 mol^{-1} m^3 cm^{-1}); UV/Vis (MeOH): $\lambda(\varepsilon)=378$ nm (29400 mol^{-1} m^3 cm^{-1}), 340 (64200 mol^{-1} m^3 cm^{-1}); MS (70 eV): *m/z* (%): 419 (100) $[M]^+$, 106 (7) $[MePyr]^+$; HRMS: *m/z* calcd for $C_{27}H_{25}N_5$: 419.2110; found: 419.2108; elemental analysis calcd (%) for $C_{27}H_{25}N_5{\cdot}1.2H_20$: C 73.51, H 6.26, N 15.87; found C 73.31, H 6.21, N 15.96.

Synthesis of complex 1b-Cu_2^{III}: $Cu(OAc)_2$ (23 mg, 0.12 mmol) was added to a solution of **2b** (10 mg, 0.024 mmol) in THF (5 mL). The mixture was stirred for 1 h at 60°C and the solvent was removed in vacuo. Then the solid was dissolved in $CHCl_3$ (10 mL). The resulting solution was filtered through cotton and evaporated to dryness. The powder was again dissolved in $CHCl_3$ (1 mL) and dry MeOH was added slowly to form two distinct layers. After one week at room temperature, the microcrystals that had formed were collected by filtration and dried under vacuo.

Acknowledgements

This work was supported by an ANR grant (Project # ANR-09-BLAN-0082-01; financial support and predoctoral fellowship for C.A.). A.T.-R. thanks the MENRT for a PhD fellowship. T.D. thanks the CNRS for support as a research fellow engineer, D.D. thanks the CNRS, la Ligue contre le Cancer association, and the cancéropôle Grand Ouest for funding and biological evaluation facilities. D.J. thanks the Belgian National Fund for Scientific Research for his research associate position. The theoretical calculations were partially performed on the Interuniversity Scientific Computing Facility (ISCF), installed at the Facultés Universitaires Notre-Dame de la Paix (Namur, Belgium), for which D. J. gratefully acknowledges the financial support of the FNRS-FRFC and the Loterie Nationale for the convention number 2.4578.02 and of the FUNDP.

[1] a) J. F. Morin, M. Leclerc, D. Ades, A. Siove, *Macromol. Rapid Commun.* **2005**, *26*, 761–778; b) C. J. Shi, Y. Wu, W. J. Zeng, Y. Q. Xie, K. X. Yang, Y. Cao, *Macromol. Chem. Phys.* **2005**, *206*, 1114–1125; c) J. Roncali, *Chem. Soc. Rev.* **2005**, *34*, 483–495; d) K. A. Hansford, S. A. Perez Guarin, W. G. Skene, W. D. Lubell, *J. Org. Chem.* **2005**, *70*, 7996–8000; e) A. Moliton, R. C. Hiorns, *Polym. Int.* **2004**, *53*, 1397–1412; f) A. J. Heeger, *Angew. Chem.* **2001**, *113*, 2660–2682; *Angew. Chem. Int. Ed.* **2001**, *40*, 2591–2611; g) Y. Shirota, *J. Mater. Chem.* **2000**, *10*, 1–25.

[2] a) B. A. Trofimov, A. M. Vasil′tsov, E. Y. Schmidt, N. V. Zorina, A. V. Afonin, A. I. Mikhaleva, K. B. Petrushenko, I. A. Ushakov, L. B. Krivdin, V. K. Belsky, L. I. Bryukvina, *Eur. J. Org. Chem.* **2005**, 4338–4345; b) J. Soloducho, S. Roszak, A. Chyla, K. Tajchert, *New J. Chem.* **2001**, *25*, 1175–1181; c) B. Tsuie, J. L. Reddinger, G. A. Sotzing, J. Soloducho, A. R. Katritzky, J. R. Reynolds, *J. Mater. Chem.* **1999**, *9*, 2189–2200; d) U. Geissler, M. L. Hallensleben, N. Rohde, *Synth. Met.* **1997**, *84*, 173–174; e) G. A. Sotzing, J. L. Reddinger, A. R. Katritzky, J. Soloducho, R. Musgrave, J. R. Reynolds, P. J. Steel, *Chem. Mater.* **1997**, *9*, 1578–1587; f) G. Pagani, A. Berlin, A. Canavesi, G. Schiavon, S. Zecchin, G. Zotti, *Adv. Mater.* **1996**, *8*, 819–823; g) U. Geissler, M. L. Hallensleben, N. Rohde, *Macromol. Chem. Phys.* **1996**, *197*, 2565–2576.

[3] D. Martineau, P. Gros, M. Beley, Y. Fort, *Eur. J. Inorg. Chem.* **2004**, 3984–3986.

[4] a) G. W. Bates, Triyanti, M. E. Light, M. Albrecht, P. A. Gale, *J. Org. Chem.* **2007**, *72*, 8921–8927; b) J. L. Sessler, G. D. Pantos, P. A. Gale, M. E. Light, *Org. Lett.* **2006**, *8*, 1593–1596.

[5] a) M. Bröring, S. Link, C. D. Brandt, E. C. Tejero, *Eur. J. Inorg. Chem.* **2007**, 1661–1670; b) T. J. Rivers, T. W. Hudson, C. E. Schmidt, *Adv. Funct. Mater.* **2002**, *12*, 33–37; c) X. Y. Cui, V. A. Lee, Y. Raphael, J. A. Wiler, J. F. Hetke, D. J. Anderson, D. C. Martin, *J. Biomed. Mater. Res. Part A* **2001**, *56*, 261–272; d) J. H. Collier, J. P. Camp, T. W. Hudson, C. E. Schmidt, *J. Biomed. Mater. Res. Part A* **2000**, *50*, 574–584.

[6] a) S. J. Schmidtke, L. A. MacManus-Spencer, J. J. Klappa, T. A. Mobley, K. McNeill, D. A. Blank, *Phys. Chem. Chem. Phys.* **2004**, *6*, 3938–3947; b) L. A. MacManus-Spencer, S. J. Schmidtke, D. A. Blank, K. McNeill, *Phys. Chem. Chem. Phys.* **2004**, *6*, 3948–3957; c) M. A. Muñoz, M. Galán, L. Gómez, C. Carmona, P. Guardado, M. Balón, *Chem. Phys.* **2003**, *290*, 69–77.

[7] B. A. Merrill, E. LeGoff, *J. Org. Chem.* **1990**, *55*, 2904–2908.

[8] G. Zotti, S. Zecchin, G. Schiavon, A. Berlin, G. Pagani, M. Borgonovo, R. Lazzaroni, *Chem. Mater.* **1997**, *9*, 2876–2886.

[9] a) G. A. Sotzing, J. R. Reynolds, A. R. Katritzky, J. Soloducho, S. Belyakov, R. Musgrave, *Macromolecules* **1996**, *29*, 1679–1684; b) J. R. Reynolds, A. R. Katritzky, J. Soloducho, S. Belyakov, G. A. Sotzing, M. Pyo, *Macromolecules* **1994**, *27*, 7225–7227; c) F. Lucchesini, *Tetrahedron* **1992**, *48*, 9951–9966; d) N. Engel, W. Steglich, *Angew. Chem.* **1978**, *90*, 719–720; *Angew. Chem. Int. Ed. Engl.* **1978**, *17*, 676–676.

[10] a) D. L. Boger, C. E. Brotherton-Pleiss, *Advances in Cycloaddition, Vol. 2* (Ed.: D. P. Curran), Jai Press, Greenwitch, **1990**; b) D. L. Boger, M. Patel, *Progress in Heterocyclic Chemistry, Vol. 1* (Eds.: H. Suschitzky, E. F. V. Scriven), Pergamon Press, Oxford, **1989**; c) D. L. Boger, *Strategies and Tactics in Organic Synthesis Vol. 2* (Ed.: T. Lindberg), Academic Press, New York, **1988**; d) D. L. Boger, *Tetrahedron* **1983**, *39*, 2869–2939.

[11] a) H. Bakkali, C. Marie, A. Ly, C. Thobie-Gautier, J. Graton, M. Pipelier, S. Sengmany, E. Léonel, J. Y. Nédélec, M. Evain, D. Dubreuil, *Eur. J. Org. Chem.* **2008**, 2156–2166; b) D. Dubreuil, M. Pipelier, H. Bakkali, J.-P. Pradère, P. Le Pape, T. Delaunay, A. Tabatchnik, CNRS International Patent, WO 2008/012440, **2008**; c) D. Dubreuil, M. Pipelier, H. Bakkali, C. Thobie, J.-P. Pradère, E. Léonel, J.-Y. Nédélec, S. Sengmany, T. Delaunay, A. Tabatchnik, CNRS International PatentWO 2008/012441, **2008**; d) S. Naud, M. Pipelier, G. Viault, A. Adjou, F. Huet, S. Legoupy, A. M. Aubertin, M. Evain, D. Dubreuil, *Eur. J. Org. Chem.* **2007**, 3296–3310; e) U. Joshi, S. Josse, M. Pipelier, F. Chevallier, J. P. Pradère, R. Hazard, S. Legoupy, F. Huet, D. Dubreuil, *Tetrahedron Lett.* **2004**, *45*, 1031–1033; f) G. T. Manh, R. Hazard, A. Tallec, J. P. Pradère, D. Dubreuil, M. Thiam, L. Toupet, *Electrochim. Acta* **2002**, *47*, 2833–2841.

[12] L. A. Cuccia, E. Ruiz, J. M. Lehn, J. C. Homo, M. Schmutz, *Chem. Eur. J.* **2002**, *8*, 3448–3457.

[13] K. T. Potts, K. A. G. Raiford, M. Keshavarz-K, *J. Am. Chem. Soc.* **1993**, *115*, 2793–2807.

[14] a) M. Darabantu, L. Boully, A. Turck, N. Ple, *Tetrahedron* **2005**, *61*, 2897–2905; b) R. T. Lewis, W. P. Blackaby, T. Blackburn, A. S. R. Jennings, A. Pike, R. A. Wilson, D. J. Hallett, S. M. Cook, P. Ferris, G. R. Marshall, D. S. Reynolds, W. F. A. Sheppard, A. J. Smith, B. Sohal, J. Stanley, S. J. Tye, K. A. Wafford, J. R. Atack, *J. Med. Chem.* **2006**, *49*, 2600–2610; c) J. Rewinkel, M. Enthoven, I. Golstein, M. van der Rijst, A. Scholten, M. van Tilborg, D. de Weys, J. Wisse, H. Hamersma, *Bioorg. Med. Chem.* **2008**, *16*, 2753–2763.

[15] Halogenopyridazines **10a–c** were synthesized through Negishi cross-coupling between the 3-chloro-6-iodopyridazine and the appropriate pyridyl zinc reagents **12a–c**.

[16] W. J. Coates, A. McKillop, *Synthesis* **1993**, 334–342.

[17] a) Stannyl pyridines **10a–c** were prepared by following the Lehn procedure from the corresponding bromopyridine (H. Nierengarten, J. Rojo, E. Leize, J. M. Lehn, A. Van Dorsselaer, *Eur. J. Inorg. Chem.* **2002**, 573–579). b) 2-Bromopyridine and 2-bromo-6-methylpyridine are commercially available, and 2-bromo-4,6-dimethylpryridine was synthesized from 2-amino-4,6-dimethylpryridine according to the Schubert protocol (U. S. Schubert, C. Eschbaumer, M. Heller, *Org. Lett.* **2000**, *2*, 3373–3376).

[18] a) R. Dorta, L. Konstantinovski, L. J. W. Shimon, Y. Ben-David, D. Milstein, *Eur. J. Inorg. Chem.* **2003**, 70–76; b) M. J. Plater, M. R. S. Foreman, J. M. S. Skakle, *J. Chem. Crystallogr.* **2000**, *30*, 535–537; c) P. N. W. Baxter, J. M. Lehn, G. Baum, D. Fenske, *Chem. Eur. J.* **2000**, *6*, 4510–4517.

[19] D. S. Chekmarev, A. E. Stepanov, A. N. Kasatkin, *Tetrahedron Lett.* **2005**, *46*, 1303–1305.

[20] a) C. Perez-Balado, A. Willemsens, D. Ormerod, W. Aelterman, N. Mertens, *Org. Process Res. Dev.* **2007**, *11*, 237–240; b) A. S. Bhano Prasad, T. M. Stevenson, J. R. Citineni, V. Nyzam, P. Knochel, *Tetrahedron* **1997**, *53*, 7237–7254.

[21] Contrary to **1b** and **1c**, **1a** was produced in very low yields (<5%) and purified with great difficulty, so our procedure is not better than another Paal–Knoor approach proposed by Jones et al. for compound **1a**. However, the tricky preparation of the 1,4-diketo precursor (15% yield) from 2,6-diacetylpyridine appeared inadequate for our purpose: R. A. Jones, M. Karatza, T. N. Toro, P. U. Civcir, A. Franck, O. Ozturk, J. P. Seaman, A. P. Whitmore, D. J. Williamson, *Tetrahedron* **1996**, *52*, 8707–8724.

[22] A. Tabatchnik, V. Blot, M. Pipelier, D. Dubreuil, E. Renault, J. Y. Le Questel, *J. Phys. Chem. A* **2010**, *114*, 6413–6422.

[23] a) M. J. G. Peach, C. R. Le Sueur, K. Ruud, M. Guillaume, D. J. Tozer, *Phys. Chem. Chem. Phys.* **2009**, *11*, 4465–4470; b) D. Jacquemin, V. Wathelet, E. A. Perpete, C. Adamo, *J. Chem. Theory Comput.* **2009**, *5*, 2420–2435.

[24] J. W. Eastman, *Photochem. Photobiol.* **1967**, *6*, 55–72.

[25] J. R. Lakowicz in *Principles of Fluorescence Spectroscopy*, Springer, Heidelberg, **2006**.
[26] H. Nierengarten, J. Rojo, E. Leize, J. M. Lehn, A. Van Dorsselaer, *Eur. J. Inorg. Chem.* **2002**, 573–579.
[27] Y. Dienes, S. Durben, T. Karpati, T. Neumann, U. Englert, L. Nyulaszi, T. Baumgartner, *Chem. Eur. J.* **2007**, *13*, 7487–7500.

Received: April 6, 2010
Published online: September 14, 2010

